15th Australasian Fluid Mechanics Conference
The University of Sydney, Sydney, Australia
13-17 December 2004

Mixing Characteristics of a Notched-Rectangular Jet and a Circular Jet

J. Mi, P. Kalt and G. J. Nathan

School of Mechanical Engineering, The University of Adelaide, South Australia 5005, Australia

Abstract

This paper reports an experimental investigation of the near-field mixing characteristics of two single air/air turbulent jets issuing, respectively, from a notched-rectangular orifice and a circular orifice with identical opening areas. Planar particle image velocimetry (PIV) was used for measurements of the velocity field. Present experiments for the two jets were conducted under the same nominal conditions with the exit Reynolds number of 72,000.

Consistent with previous investigations of other noncircular jets, the notched jet is found to have an overall superior mixing capability over the circular counterpart. Immediately downstream of the nozzle exit, it entrains, and then mixes with, the surroundings at a higher rate. This jet has a shorter potential core and higher rates of decay and spread than the circular jet. The phenomenon of axis switching is also found to occur in this jet.

Introduction

Extensive research into noncircular jets has been performed in the past two decades or so (e.g., [1-21]), largely due to their potential to entrain ambient fluid more effectively than comparable circular jets. The superior mixing capability of such jets is experimentally related either to the non-uniform curvature of their initial perimeter, relative to the evenness for the circular configuration, or to the instabilities produced by the initial perimeter's sharp corners through the asymmetric distribution of pressure and mean flow field [3]. Both phenomena are deduced to accelerate three-dimensionality of the jet structures, therefore causing greater entraining and mixing. For elliptic and rectangular jets, azimuthal curvature variation of initial vortical structures produces non-uniform self-induction and three-dimensional structures. As a result, these flows spread more rapidly in the minor axis plane than in the major axis plane, causing 'axis switching' at a certain distance from the nozzle exit (e.g., [3,21]). For corner-containing configurations, the corners promote the formation of fine-scale turbulence and thus enhance fine-scale mixing [4,9]. The above experimental results have also been demonstrated in a number of numerical simulations (e.g. [1,2,12]). The review of Gutmark and Grinstein [3] summarizes both experimental and numerical studies in the context of noncircular jets.

Note however that previous investigations on noncircular jets, e.g.[1-22], have focussed predominantly on elliptical, rectangular (including square), and triangular configurations. Few detailed measurements and simulations have been performed for other shapes. Although Mi et al. [11] provided hot-wire measurements in nine different-shaped jets, their data were limited only to the centreline mean and rms of the axial velocity.

The present study carried out planar PIV measurements of two single jets issuing respectively from a circular and a four-notched rectangular orifice, with the same opening area (A) and thus an identical equivalent diameter D_e [$\equiv 2(A\pi^{-1})^{1/2}$] of approximately 12 mm (Fig. 1). The aspect ratio (AR) of the notched orifice, i.e., the ratio of the long to short axes of symmetry of the orifice cross-section, is AR = 1.5. The main objective of the present report is to compare the mean flow fields of the two jets to identify their similarity and difference.

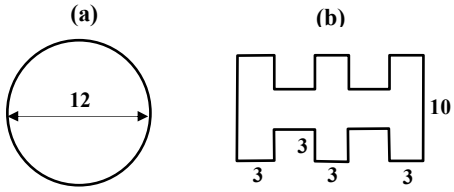

Fig. 1. Present orifice shapes and dimensions (mm). (a) Circle: D_e = D_h = 12 mm, D_e/D_h = 1 and AR = 1; (b) Notched-rectangle: D_e = 12 mm, D_h = 9.12 mm, D_e/D_h = 1.32 and AR = 1.5.

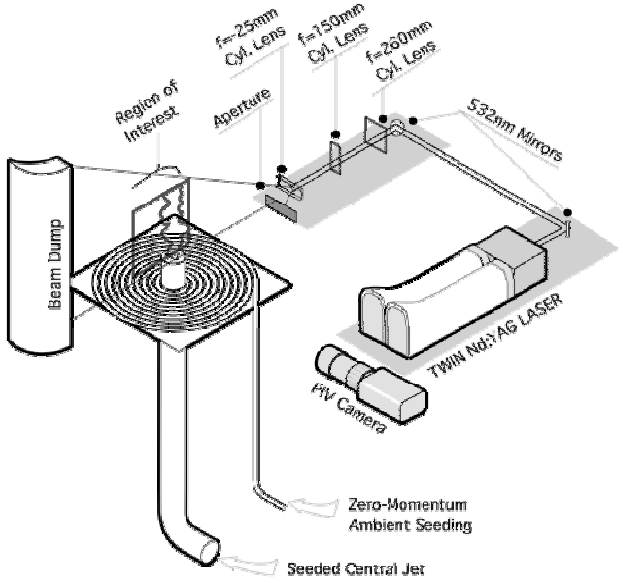

Fig. 2. Experimental set-up of the PIV system.

Experimental details

The PIV experiments were conducted at the Laser Laboratory of Turbulence, Energy & Combustion Group, The University of Adelaide. Fig. 2 shows schematically the experimental set-up. A compressor with an operating pressure of up to 650 kPa supplied conditioned air to the test rig. The two orifice plates (Fig. 1) were separately attached to the vertical tube of 25.4 mm i.d. and 1000 mm in length. The flow rate through the tube, which was used to calculate the jet exit bulk velocity and Reynolds number, was obtained by a flow meter. Good axisymmetry of the tube flow immediately upstream of each office plate attached was achieved since nearly identical and symmetric radial profiles of the mean velocity at the tube exit for different orientations (not presented here) were found. The tube flow at the exit was not fully developed so that its mean velocity profile did not follow the one-seventh power-law as for the fully-developed pipe flow. The axial turbulence intensity was about 3% at the centre and up to 26% near the tube edge. Both jets were measured at the same nominal Reynolds number of Re = 72,000, where Re $\equiv U_e D_e/\nu$,

with U_e being the exit bulk velocity, D_e the exit equivalent diameter and ν the kinematic viscosity of fluid.

The air jet flows were seeded with small olive oil droplets, with a mean diameter of about 1 μm, generated by a Laskin nozzle particle generator. This type of seeding follows the bulk flow well and is suitable for the present velocity range [16]. The droplets from the generator were divided into two streams, one used for seeding the core jet flow and the other through a plastic tube coil with fine holes upwards for seeding ambient air with very low ejecting speed (< 1% U_e). The whole rig was positioned under an extraction hood and was further surrounded by a curtain of black cloth to reduce the effects of room draughts and stray laser scattering.

PIV measurements were realised by a Quantel Brilliant Twins double-head Nd:YAG laser at a frequency of 10 Hz and power of 250 mJ per pulse at λ = 532 nm. This laser is specially designed for PIV applications, each of the laser heads being independently triggerable. The temporal separation between laser pulses was adjusted from 10 to 40 μs, depending on the flow-field. The camera is a MegaPlus ES1.0 PIV camera operated in triggered double exposure mode. The CCD in this camera is 1008 pixels wide by 1018 pixels high. The collection optics comprised a Nikon ED 70-300 m (set to 110 mm) telephoto lens coupled to the camera C-mount with an adapter. The aperture was fully opened ($f^{\#} = 4$). The imaging region was 100 mm by 100 mm, each pixel corresponding to 10 μm. Data were collected from the camera at 20 Hz into a memory buffer on the data storage computer. At the end of a run, the entire dataset of PIV image pairs were saved to hard disk for later processing.

The time delay between laser pulses was selected so that the interrogation region could be set to 32 by 32 pixels, with a 50% offset. This resulted in an effective resolution for the velocity measurements of 3 mm. The resulting vector field is comprised of FIL by FIL vectors. A 2-pass Hart correlation algorithm was used to correlate the two image pairs. The correlation image scanned for peaks using a centroid-hunting algorithm on a roaming 3x3 pixel mask. This gives sub-pixel accuracy for the determined velocity. Outliers (erroneous vectors) were detected by comparison to the neighbourhood average. Outliers were replaced by a suitable, alternative correlation peak where possible, and were otherwise replaced by interpolation from valid neighbouring vectors. This is only recommended when outlying vectors occur only infrequently within any given vector field.

Mean vector fields were found from an ensemble of 520 vector fields for each condition. Downstream measurements of the flow were made by axially translating the nozzle relative to the camera and laser sheet.

Results and discussion

Figures 3(a) and 3(b) show the mean velocity ($\langle U \rangle / U_e$) contours and mean streamlines in the two symmetric (i.e., *xy* and *xz*) planes of the notched jet, respectively, while those results obtained from the central plane of the circular jet are presented in Fig. 3(c) for comparison. We also present the mean vorticity contours in Fig. 4. The measurement area shown here is in the near-field region at $0.4 \leq x/D_e \leq 8.2$. For the notched jet, the *xy* and *xz* planes are the minor and major axis planes as indicated on the plot.

Comparison of Figs. 3(a)-(c) and 4(a)-(c) suggests significant differences in the mean flow field between the two jets. Apparently, the core (bounded with yellow contours) of the mean notched jet initially contracts over a short distance $x \leq 1.0D_e$ in the minor axis (*xy*) plane while simultaneously it spreads out in the major axis (*xz*) plane. Interestingly, in the minor axis plane, the jet 'edge' spreads very rapidly over the region $0.5 < x/D_e < 2$; further downstream, the spreading speed slows down but still remains high relative to the circular case (Fig. 3(a)). In the major

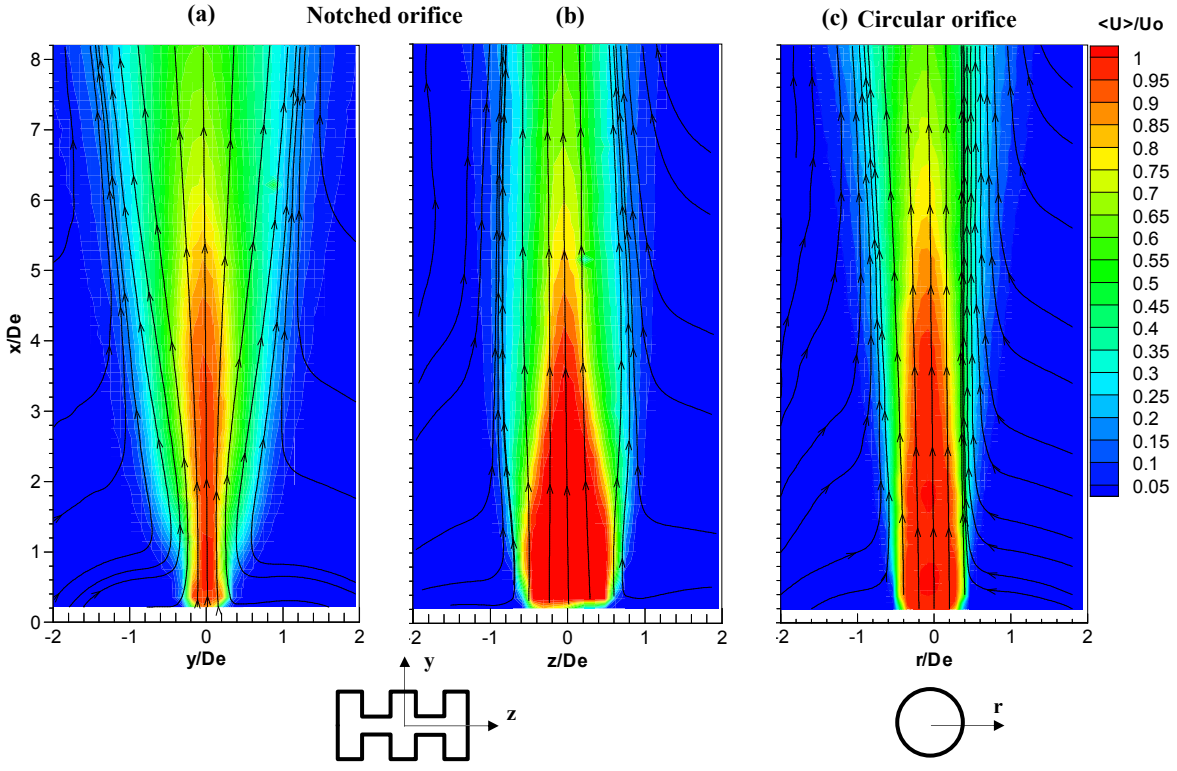

Fig. 3. Mean velocity contours and streamlines. (a) notched jet in the *xy* plane; (b) notched jet in the *xz* plane; (c) circular jet.

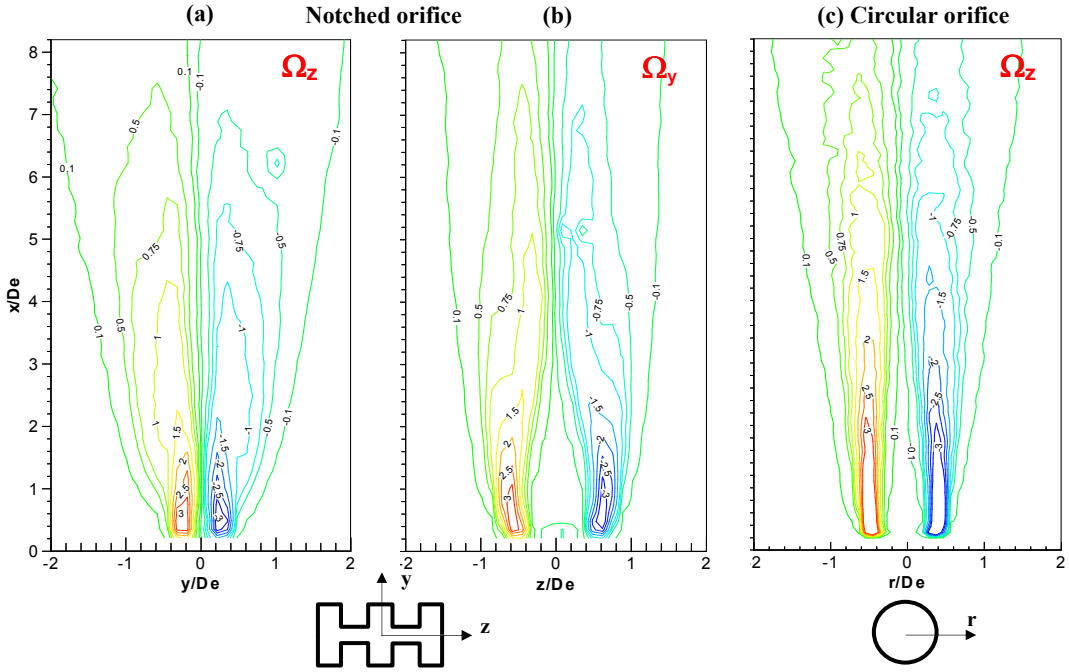

Fig. 4. Mean vorticity contours. (a) Ω_z in the *xy* plane, notched jet; (b) Ω_y in the *xz* plane, notched jet; (c) Ω_z, circular jet.

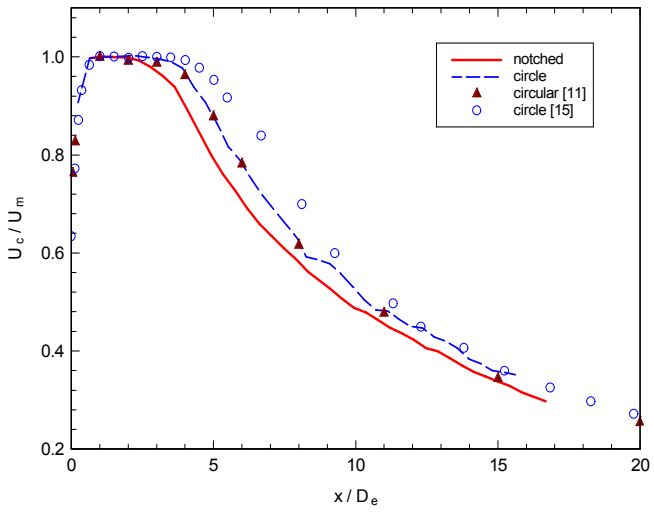

Fig. 5. Mean velocity decay along the jet centreline.

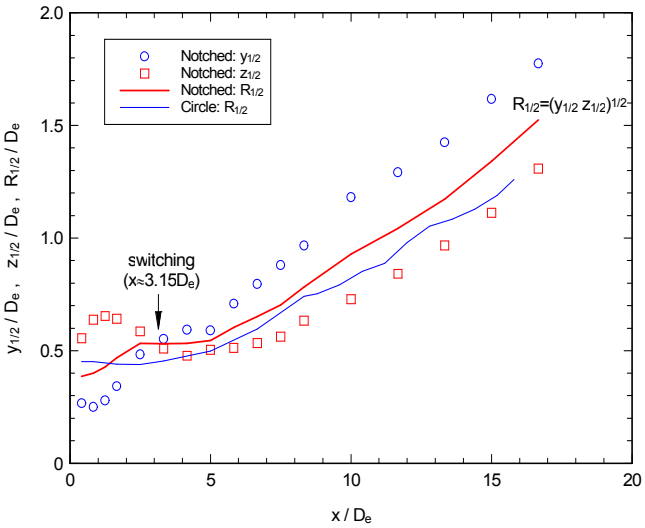

Fig. 6. Half-velocity widths of the notched jet and their comparison with the circular counterpart.

axis plane, however, the notched core jet contracts slowly from $x/D_e \approx 1.0$ to $x/D_e \approx 6.0$ and starts to spread further downstream. By comparison, the circular jet spreads out all the way in all lateral directions, yet with a relatively low rate. Moreover, as indicated by red to yellow colour scales in Figs. 3(a)-(c), the mean velocity of the notched jet decreases with x at a higher rate than that of the circular jet. It is hence clear that overall the notched jet spreads and decays more rapidly than does the circular jet. This implies that it entrains (and then mixes) ambient fluid at a higher rate. This is consistent with previous observations for other noncircular jets [3-9].

The above conclusion is made based only on the measurements in the *xy* and *xz* planes rather than for the entire field of the notched jet. However, further support for this deduction can be derived from the streamwise variations of the normalized centreline velocity, U_c / U_m, and half-velocity widths ($y_{1/2}$ and $z_{1/2}$), shown in Figs. 5 and 6. Here, U_m is the maximum of $U_c(x)$ occurring near to the orifice exit; the half-velocity width is the lateral distance from the jet axis to a location at which the mean velocity $\langle U \rangle$ is half the centreline mean velocity U_c, i.e., $\langle U \rangle = U_c/2$. The data reported in Figs. 5 and 6 were extracted from the PIV measurements over the range $0.4 \leq x/D_e < 17$. For comparison with previous work, the hot-wire data of U_c / U_m of Mi et al. [11], Re ≈ 15000, and Quinn [15], Re ≈ 200000, for a circular orifice jet are also included in Fig. 5. It is interesting to note that the present data for the circular jet agree very well with [11] while Quinn's data differ quite significantly at $x/D_e < 12$. The difference between the present results and those of [15] is likely associated with very distinct upstream flow configurations used in the two studies. While the present study utilized an industry-type pipe, without conditioning, to supply compressed airflow to the orifice, Quinn adopted a conventional jet facility, which has a large settling chamber fitted with honey-comb and mesh-wire screens and a three-dimensional contraction, to achieve a low-turbulence-intensity uniform flow upstream of the orifice.

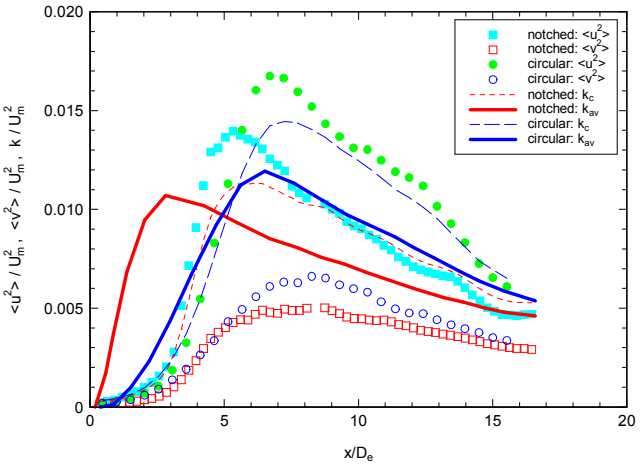

Fig. 7. Centreline distributions of the normal stresses ($\langle u^2 \rangle$, $\langle v^2 \rangle$) and turbulence kinetic energy (k_c).

The centreline velocity decreases more rapidly with axial distance (Fig. 6), while the half-velocity equivalent radius, $R_{1/2} = (y_{1/2}\, z_{1/2})^{1/2}$, spreads faster (Fig. 7), in the notched jet than in the circular jet. (Note that $R_{1/2}$ was adopted by Hussain and Husain [7] for elliptic jets.) Consistently, the potential core is shorter for the former, with length of $L_{pc} \approx 2.2D_e$, relative to $L_{pc} \approx 3.5D_e$ for the latter. Figure 6 also demonstrates that for the notched jet the half-width in the minor axis plane, $y_{1/2}$, develops from being initially smaller than that in the major axis plane, $z_{1/2}$, to exceeding the latter, i.e., $y_{1/2} > z_{1/2}$, at $x \approx 3.15D_e$. That is, there is axis-switching occurring in the notched jet with AR = 1.5, similar to rectangular jets initially with or without disturbance of tabs [21].

Figure 7 shows the centreline Reynolds normal stresses, $\langle u^2 \rangle$ and $\langle v^2 \rangle$, of the two jets, where u and v represent the axial and lateral components of the fluctuating velocity. Also reported are the centreline distributions (k_c, dashed lines) of the turbulence kinetic energy $k = (\langle u^2 \rangle + \langle v^2 \rangle + \langle w^2 \rangle)/2$ and the streamwise variations of the averaged k over the cross-section (k_{av}, solid lines). Note that k_{av} was obtained in the xy and xz planes for the notched jet while for the circular case it was estimated from the central plane. As expected, the magnitude of $\langle u^2 \rangle$ is much greater than that of $\langle v^2 \rangle$ in both jets. In the near field, as x increases, both $\langle u^2 \rangle$ and $\langle v^2 \rangle$ increases. This increase results from the high production of turbulence in the shear layers; the turbulence is then diffused from the shear layers to the jet centreline. For the notched jet, $\langle u^2 \rangle$ and $\langle v^2 \rangle$ peak at $x/D_e \approx 5.5$ and 7.5, respectively, while the corresponding peaks occur at $x/D_e \approx 7$ and 8.5 for the circular counterpart. Consequently, the kinetic energy k_c peaks nearly at the same location as $\langle u^2 \rangle$ in both jets.

One important finding extracted from Fig. 7 is that the averaged kinetic energy k_{av} evolves very distinctly in the two jets. This reflects a significant difference in their mixing mechanisms. Clearly, k_{av} grows much faster until $x/D_e \approx 3$ in the notched jet than in the circular counterpart, indicating that, in the very near region, the former jet mixes far more intensively with its surroundings. The stronger mixing is accompanied by a faster spreading of the mean velocity field, Fig. 3, and thus a shorter potential core region, Fig. 4. The overall kinetic energy k_{av} turns to decrease from $x/D_e \approx 3$ in the notched jet and much farther downstream from $x/D_e \approx 6.5$ in the circular jet. This is because large-scale coherent structures formed in the former are more three-dimensional in more complex flow patterns and have stronger interactions with each other and the ambient flow, thus breaking down faster. As a result, k is dissipated more rapidly in this jet. It follows that, downstream of x/D_e = 5-6, k is higher in the circular than notched jet.

Conclusions

In this study we carried out planar PIV measurements of two single jets issuing respectively from a circular and a notched rectangular orifice with same opening areas. Comparison has been made between the near-field mixing characteristics of the two jets. It has been found that, in general, the notched jet entrains the ambient fluid at a higher rate than does the circular counterpart. Specifically, the former jet both decays and spreads faster, yielding a shorter potential core. Immediately downstream from the nozzle exit ($x < 3.0D_e$), it mixes the surroundings much faster and, hence, the cross-sectional averaged kinetic energy grows far more rapidly relative to the circular case. In addition, the phenomenon of axis switching occurs (at $x \approx 3.15D_e$) in the notched jet.

Acknowledgment

The authors gratefully acknowledge the support of the Australian Research Council.

References

[1] Grinstein, F.F., Self-induced vortex ring dynamics in subsonic rectangular jets. *Phys. Fluids* **7**, 1995, 2519-2521.

[2] Grinstein, F.F., Gutmark, E. and Parr, T., Near field dynamics of subsonic free square jets, A computational and experimental study, *Phys. Fluids*, **7**, 1995, 1483-1497.

[3] Gutmark, E. & Grinstein, F. F., Flow control with noncircular jets. *Ann. Rev. Fluid Mech*., **31**, 1999, 239-272.

[4] Gutmark, E., Schadow, K.C., Parr, T.P., Hanson-Parr, D.M., & Wilson, K.J., Noncircular jets in combustion systems, *Expts Fluids* **7**, 1989, 248-258.

[5] Ho, C.M. & Gutmark, E., Vortex induction and mass entrainment in a small-aspect-ratio elliptic jet, *J. Fluid Mech*. **179,** 1987, 383-405

[6] Husain H. S. & Hussain F., Controlled excitation of elliptic jets *Phys. Fluids* **26,** 1983, 2763-2766

[7] Hussain, F. and Husain, H.S., Elliptic jets. Part 1. Characteristics of unexcited and excited jets, *J. Fluid Mech*. **208**, 1989, 257-320.

[8] Husain, H.S. and Hussain, F., Elliptic jets. Part 2. Dynamics of coherent structures: paring, *J. Fluid Mech*. **233**, 1991, 439.

[9] Koshigoe, S., Gutmark, E. & Schadow, K., Initial development of non-circular jets leading to axis switching, *AIAA J*. **27**, 1989, 411.

[10] Krothapalli, A., Baganoff, D. & Karamcheti, K., On the mixing of rectangular jets. *J. Fluid Mech*. **107**, 1981, 201-220.

[11] Mi, J. Nathan, G.J. and Luxton, R.E., Centreline mixing characteristics of jets from nine differently shaped nozzles, *Expts. Fluids* **28**, 2000, 93-94.

[12] Miller, R.S., Madnia, C.K. and Givi, P., Numerical simulation of non-circular jets, *Computers & Fluids* **24**, 1995, 1-25.

[13] Quinn, W.R., On mixing in an elliptic turbulent free jet, *Phys. Fluids* **A1**, 1989, 1716-1722.

[14] Quinn, W.R., Mean flow and turbulence measurements in a triangular turbulent free jet, *Int. J. Heat & Fluid Flow* **11**, 1990, 220-224.

[15] Quinn, W.R., Development of a large-aspect-ratio rectangular turbulent free jet, *AIAA J*. **32**, 1994, 547-554.

[16] Raffel M., Willert C. & Kompenhans J., *Particle image velocimetry –A Practical Guide*, Springer, Germany, 1998.

[17] Schadow, K.C., Gutmark, E., Parr, D.M. and Wilson, K.J., Selective control of flow coherence in triangular jets, *Expts. Fluids* **6**, 1988, 129-135.

[18] Sforza, P.M., Steiger, M.H. and Trentacoste, N., Studies on three dimensional viscous jets, *AIAA J*. **4**, 1966, 800.

[19] Trentacoste, N. and Sforza, P.M., Further experimental results for three dimensional free jets, *AIAA J*. **5**, 1967, 885.

[20] Tsuchiya, Y., Horikoshi, C. and Sato, T, On the spread of rectangular jets, *Exps. Fluids* **4**, 1986, 197-204.

[21] Zaman, K.B.M.Q., Axis switching and spreading of an asymmetric jet: the role of coherent structure dynamics, *J. Fluid Mech*. **316**, 1996, 1-27.

[22] Zaman, K.B.M.Q., Spreading characteristics of compressible jets from nozzles of various geometries, *J. Fluid Mech*. **383**, 1999, 197-228.